Available online at www.sciencedirect.com
ScienceDirect
Journal of Sound and Vibration 299 (2007) 786–805
JOURNAL OF SOUND AND VIBRATION
www.elsevier.com/locate/jsvi

Monitoring a delamination in a laminated composite beam using in-situ measurements and parametric identification

Christophe Bois, Philippe Herzog*, Christian Hochard

Laboratoire de Mécanique et d'Acoustique, CNRS, 31, chemin Joseph Aiguier, 13402 Marseille cedex 20, France

Received 20 December 2004; received in revised form 28 June 2006; accepted 13 July 2006

Abstract

A method is described for monitoring a single delamination in a laminated composite plate. The dynamic response of the structure is obtained via the electromechanical impedance of a piezoelectric transducer cemented onto the structure. We focus here on the coupling with bending modes using thin devices which can be embedded in the material during the manufacturing process. A model including the delamination as well as the transducer is presented. The geometrical parameters of the delaminated zone are identified by comparing the modal parameters calculated from impedance measurements with those obtained using our model. Upon applying this method of identification to a test laminated beam, the length and position of several delaminations were estimated to within 15%.

1. Introduction

The anisotropy and lack of homogeneity of composite materials result in various and complex damage mechanisms. In a composite structure, one can observe micro-cracking (micro-decoherence processes and micro-cracks), ply fractures (transverse cracks), delaminations, and laminate fractures. Many authors have proposed models for predicting the evolution of these damage processes (see Refs. [1,2]). Since these damage mechanisms are interrelated, however, a 3D modelling procedure is often necessary (see Ref. [3]). Approaches of this kind are not easily applicable in industrial context. Moreover, in the case of classical static or fatigue loading conditions, the uncertainties about the boundary conditions and the imperfections of the model can have considerable effects. In order to reduce the need for wide safety margins and optimise structure design, suitable methods have therefore become necessary for detecting and characterising each type of damage. With methods of this kind, predictive models could be used to determine whether the damage is still acceptable or whether repair operations are required.

In order to reduce time-consuming ground maintenance work, we have been investing the possibility of an onboard system of measurement. Several sensors can be used to carry out measurements of this kind, such as piezoelectric transducers (see Ref. [4]), the composite carbon fibre components themselves (electrical resistance measurements) (see Refs. [5–7]), and optical fibres (see Refs. [8,9]). We decided to use piezoelectric transducers

*Corresponding author. Tel.: +33 491 164089; fax: +33 491 164080.
E-mail address: herzog@lma.cnrs-mrs.fr (P. Herzog).

0022-460X/$ - see front matter © 2006 Elsevier Ltd. All rights reserved.
doi:10.1016/j.jsv.2006.07.026

for several reasons. First, Lin and Chang (see Ref. [10]) have established that thin piezoceramic layers can be embedded in composite laminates during the manufacturing process without degrading the structural integrity of the host composite structures. In addition, devices of this kind make it possible to perform both ultrasonic and modal analysis. Many authors have used thin piezoelectric transducers to generate and receive Lamb's waves in composite plates in order to monitor an impact or other causes of local degradation (see Refs. [11,12]). These devices have been less commonly used to determine the modal response of a structure, although modal analysis has been used for several decades to detect and characterise damage in structures (see Refs. [13–16]). Diaz Valdes and Soutis [17] used thin piezoceramic elements and measured resonance peak shifts in order to detect and monitor the evolution of a delamination process in a composite beam. These authors could only assess the defect qualitatively because they did not use a model describing the delamination.

Ling et al. [18] proposed a model for identifying a delamination. Their model allow to compute eigenvalues for a delaminated composite beam, but, as actuators and sensors are not taken into account, their model cannot estimate the amplitudes of the modes.

Keilers and Chang [19,20] proposed a model taking into account the sensors and actuators (piezoceramic transducers). In this way, they can perform a parametric identification of a delamination in composite beam. But their model was limited to symmetrical beams (two transducers on opposite faces and a delamination on the neutral axis).

In this paper, we propose a general method which does not require making any assumptions about the symmetry of the laminate, the delamination or the position of the transducer.

First we present the method of measurement used for this purpose and describe a general model which was specially adapted to the use of a thin piezoelectric transducer for analysing the electromechanical coupling. In the second part, an electromechanical model based on laminate theory is developed for dealing with delaminated beam structures. In the third part, this model is used to characterise a delamination. Experimental and simulated modal parameters are obtained for a few modes, using a mean squares estimate technique. Comparisons between modal parameters make it possible to determine the geometrical parameters characterising the delamination.

2. Electromechanical impedance measurement

2.1. General principle

Mechanical impedance measurements have been used for several decades to determine the modal response of structures. These measurements generally involve the use of electrodynamic or hydraulic shakers as actuators. Accelerometers or laser vibrometers are then used to detect the response of the structure under investigation.

As our aim was to make embedded measurement, we used thin actuators and receivers which could be included in the structure during their manufacture. Some authors proposed to use fibre optic sensors to measure vibration modes of structures (see Ref. [18]). This technique needs an actuator for generating vibration, and seems therefore unpractical except in a laboratory context. Other authors proposed to use piezoelectric transducers in the form of thin discs (see Refs. [4,10]). These transducers can play the role of both actuator and receiver. A single transducer can thus be used to carry out electromechanical impedance measurements.

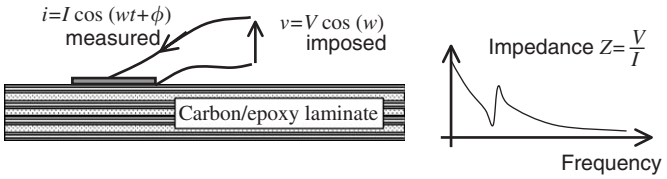

Fig. 1. Principle of the electromechanical impedance measurement.

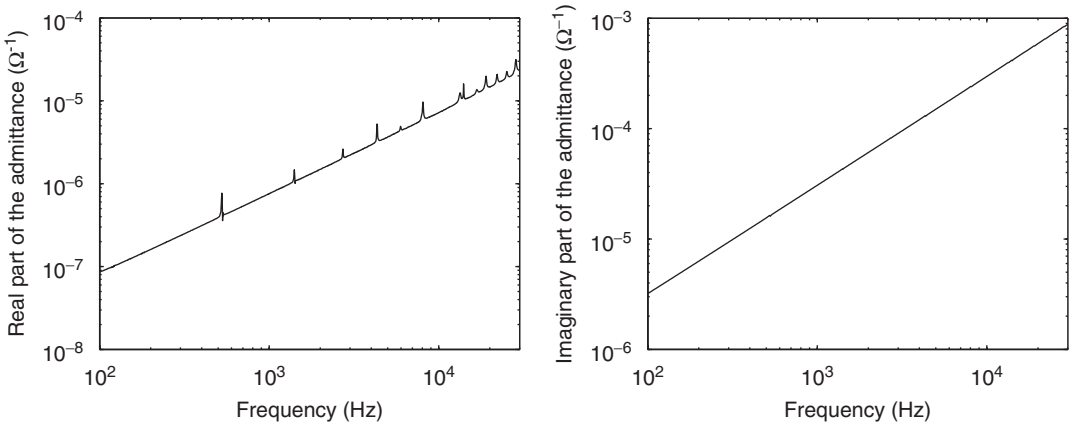

Fig. 2. Example of an electromechanical impedance measurement. Real part and imaginary part.

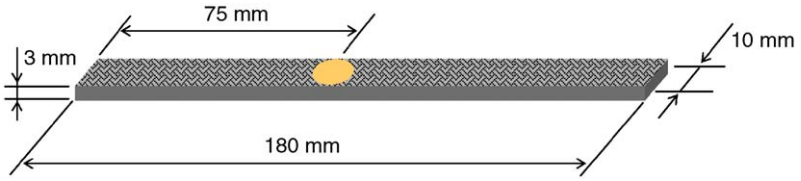

Fig. 3. Characteristics of the laminated beam made of 16 carbon/epoxy unidirectional plies $[45^\circ, -45^\circ, 90^\circ, 0^\circ]_{2S}$.

Fig. 1 shows the basic idea underlying this method of measurement: a sinusoidal tension is fed between the terminals of the transducer, and the electrical current reaching the transducer is measured. Fig. 2 gives an example of an electromechanical impedance measurement carried out on the laminated beam presented in Fig. 3. The real part of the impedance shows a series of peaks corresponding to the bending modes of the structure. We can also see the capacitive behaviour of the piezoelectric material, which results in a linear evolution (in log–log scales) on the impedance versus frequency graph. This measurement therefore provides information about both the electrical behaviour of the piezoelectric disc and the mechanical behaviour of the whole structure.

2.2. A general electromechanical model for thin transducers

The aim of this part of the study was to develop a simple linear model which could be used to analyse the electromechanical coupling. This analysis will subsequently be used to process the impedance measurements in the last part of the study.

Ling and Xie [21] proposed a method of extracting the mechanical impedance from the impedance measurement using a piezoceramic inertial actuator. These authors assumed the transducer to be attached at a single point to the structure because an inertial transducer generates a force perpendicular to the contact surface. Here we used thin transducers mainly generating forces running parallel to the contact surface. The force distribution over the contact surface consequently has to be taken into account. We therefore decided to develop a general model assuming only that the thickness of the piezoelectric transducer is much smaller than its other dimensions.

Let us consider the piezoelectric structure described in Fig. 4. We take an electric potential V equal to zero at the negative terminal. We want to calculate the electrical admittance defined by

$$Y = \frac{I}{V^+}, \tag{1}$$

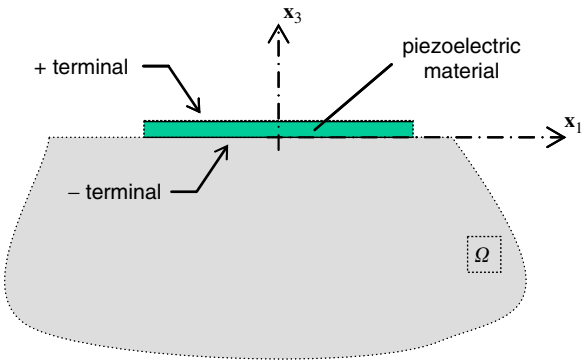

Fig. 4. Piezoelectric structure.

where V^+ is the electric potential assumed to be uniform over the positive terminal and I is the electrical current flowing into the positive terminal. Assuming that a sinewave excitation is reaching the transducer with an angular frequency ω, I can be calculated straightforwardly from the surface electric charge displacement Q of the positive terminal:

$$I = \int_{+\text{ terminal}} \dot{Q}\,\mathrm{ds} = \mathrm{j}\omega \int_{+\text{ terminal}} Q\,\mathrm{ds}. \tag{2}$$

In our application, the piezoelectric material is quite thin in comparison with its width (thickness 0.15 mm, width 10 mm). The electrical field $\mathbf{E}$ and the electric charge displacement $\mathbf{D}$ are therefore almost parallel to the $\mathbf{x}_3$ direction. In addition, we can assume the electrical field to be constant with x_3, leading to

$$V = \frac{x_3}{h_p} V^+ \exp(\mathrm{j}\omega t), \tag{3}$$

$$E_1 = 0, \quad E_2 = 0 \quad \text{and} \quad E_3 = \frac{V^+ \exp(\mathrm{j}\omega t)}{h_p}, \tag{4}$$

where h_p is the thickness of the piezoelectric transducer.

An arbitrary finite elements discretisation procedure was used in order to obtain an analytic expression for the admittance.

Appendix A gives details of the method used to calculate the discretised equations giving the electromechanical problem, which lead to the following equation:

$$\begin{cases} (\mathbf{K} - \omega^2\mathbf{M})\mathbf{U} - \mathbf{P}V^+ = 0, \\ \mathbf{P}^{\mathrm{T}}\mathbf{U} + CV^+ = \dfrac{I}{\mathrm{j}\omega}, \end{cases} \tag{5}$$

where $\mathbf{U}$ is the column vector of nodal displacements, $\mathbf{K}$ the stiffness matrix, $\mathbf{M}$ the mass matrix, $\mathbf{P}$ the column matrix of electromechanical coupling, and C the electric capacity. C is defined by

$$C = \frac{S\varepsilon_{33}^{\varepsilon}}{h_p}, \tag{6}$$

where S is the area of the positive terminal, and $\varepsilon_{33}^{\varepsilon}$ the dielectric constant at constant strain field in the 3–3 direction.

Because of our electrical assumption, the only electrical degree of freedom (dof) is V^+, and $\mathbf{P}$ is thus a column matrix.

By substituting $\mathbf{U}$ into Eq. (5) we obtain

$$[\mathbf{P}^{\mathrm{T}}(\mathbf{K} - \omega^2\mathbf{M})^{-1}\mathbf{P} + C]V^+ = \frac{I}{\mathrm{j}\omega}. \tag{7}$$

Eqs. (1) and (7) can be used to determine the admittance Y:

$$Y = j\omega[\mathbf{P}^{T}(\mathbf{K} - \omega^2\mathbf{M})^{-1}\mathbf{P} + C]. \tag{8}$$

From the expression for the admittance given by Eq. (8), we can extract what we call the total capacity C_T:

$$C_T = \mathbf{P}^{T}(\mathbf{K} - \omega^2\mathbf{M})^{-1}\mathbf{P} + C. \tag{9}$$

In this expression, we can see the dynamical stiffness matrix $\mathbf{K} - \omega^2\mathbf{M}$. As in the case of the mechanical impedance, the scalar values measured makes it possible to trace the dynamical behaviour of the whole structure. $\mathbf{P}$ serves as a projector by translating the electromechanical coupling (Newtons/Volt). It depends on the position of the transducer and the piezoelectric coefficients. C is theoretically constant, but in the experimental data, C changes slightly with the frequency (see Ref. [22]).

3. Analytic model for a delaminated beam with a piezoelectric transducer

Simplified models taking the presence of a piezoelectric transducer into account are already available (see Ref. [23]). Most of the authors in question have modelled symmetrical beams, that is to say beams having two transducers on opposite faces, in order to isolate the bending modes involved (see Refs. [18,24,25,28]). Transducers are usually modelled by an actuator attached to the structure at two points (see Ref. [26]). To obtain more accurate modelling, we have adapted the laminate theory by simulating a piezoelectric ply. A similar approach has been used in the field of active vibrations control (see Ref. [27]). This approach, which makes it possible to obtain an analytic model for beam structures, can be adapted to plate structures using the finite elements method.

To model the delamination, one of the most usual methods consists in cutting out the structure in several parts, in order to isolate the delamination (see Ref. [29]). The interface equilibrium equations then yield a global model. Cho and Kim [30] have proposed a general formulation based on distribution theory, which they applied to plates using the finite elements method.

Keilers and Chang [19] described a model accounting for both the transducer and the delamination, which was valid only in the case of symmetrical beams. Here we therefore propose a more general model which is suitable for general cases.

A previous study by one of the present authors (see Ref. [31]) was based on a classical beam theory (uniaxial stress), applied to a quasi-isotropic laminate. This theory is not suitable for dealing with laminates, however, as the anisotropy of composite materials and differences in orientation between the plies generate radial stresses on the ply scale. This leads to a 5% error in the resonance frequencies, which can be avoided with the more general model presented here.

3.1. Theory for piezoelectric laminates—application to bending modes of a composite beam

In plane stress, let us define the stress vector $\boldsymbol{\sigma}$ and the strain vector $\boldsymbol{\varepsilon}$ as follows:

$$\boldsymbol{\sigma} = \begin{bmatrix} \sigma_{11} \\ \sigma_{22} \\ \sigma_{12} \end{bmatrix} \quad \text{and} \quad \boldsymbol{\varepsilon} = \begin{bmatrix} \varepsilon_{11} \\ \varepsilon_{22} \\ 2\varepsilon_{12} \end{bmatrix}. \tag{10}$$

In the case of an elastic, not piezoelectric material, the constitutive law can be written:

$$\boldsymbol{\varepsilon} = \mathbf{S}\boldsymbol{\sigma}, \tag{11}$$

where $\mathbf{S}$ is the flexibility tensor.

For example, in the case of an orthotropic material:

$$\mathbf{S} = \begin{bmatrix} \frac{1}{E_1} & -\frac{v_{21}}{E_2} & 0 \\ -\frac{v_{21}}{E_2} & \frac{1}{E_2} & 0 \\ 0 & 0 & \frac{1}{G_{12}} \end{bmatrix}, \tag{12}$$

where E_1 is the longitudinal Young's modulus, E_2 is the transversal Young's modulus, G_{12} is the shear modulus, and v_{21} is the Poisson's ratio.

In the case of a piezoelectric material, the 3D constitutive laws are as follows, when the stress $\boldsymbol{\sigma}$ and the electrical field $\mathbf{E}$ are taken to be independent variables:

$$\varepsilon_{kl} = S^E_{klij}\sigma_{ij} + d_{klq}E_q, \tag{13}$$

$$D_p = d_{pij}\sigma_{ij} + \varepsilon^\sigma_{pq}E_q, \tag{14}$$

where $\boldsymbol{\varepsilon}^\sigma$ is the dielectric tensor at constant stress field, $\mathbf{S}^E$ is the flexibility tensor at constant electrical field, and $\mathbf{d}$ is the corresponding piezoelectric coupling tensor.

With the same assumptions as those involved in Eq. (4), the constitutive laws given by Eqs. (13) and (14) can be written in plane stress terms with an uniaxial electric field in the form:

$$\boldsymbol{\varepsilon} = \mathbf{S}^E\boldsymbol{\sigma} + \mathbf{d}E_3, \tag{15}$$

$$D_3 = \mathbf{d}^{\mathrm{T}}\boldsymbol{\sigma} + \varepsilon^\sigma_{33}E_3, \tag{16}$$

where

$$\mathbf{d} = \begin{bmatrix} d_{113} \\ d_{223} \\ d_{123} \end{bmatrix}. \tag{17}$$

By extracting $\boldsymbol{\sigma}$ from Eq. (15), we obtain

$$\boldsymbol{\sigma} = (\mathbf{S}^E)^{-1}(\boldsymbol{\varepsilon} - \mathbf{d}E_3) \tag{18}$$

and by substituting it into Eq. (16), we obtain

$$D_3 = \mathbf{d}^{\mathrm{T}}(\mathbf{S}^E)^{-1}\boldsymbol{\varepsilon} + (\varepsilon^\sigma_{33} - \mathbf{d}^{\mathrm{T}}(\mathbf{S}^E)^{-1}\mathbf{d})E_3. \tag{19}$$

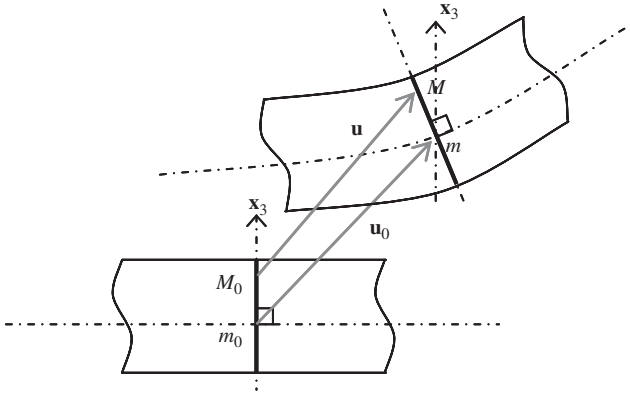

Fig. 5. Kirchhoff–Love's displacement field.

Eqs. (18) and (19) are therefore the constitutive laws under plane stress conditions, where $\boldsymbol{\varepsilon}$ and E_3 are independent variables.

We took a Kirchhoff–Love's displacement field illustrated in Fig. 5, defined by

$$\mathbf{u} = \mathbf{u}^0 - x_3 \mathbf{grad}(u_3^0), \tag{20}$$

where $\mathbf{u}^0$ is the displacement of the point m^0.

The strain vector defined by Eq. (10) can then be written in the form:

$$\boldsymbol{\varepsilon} = \boldsymbol{\varepsilon}^0 + x_3 \mathbf{K}, \tag{21}$$

with:

$$\boldsymbol{\varepsilon}^0 = \begin{bmatrix} u_{1,1}^0 \\ u_{2,2}^0 \\ u_{1,2}^0 + u_{2,1}^0 \end{bmatrix} \quad \text{and} \quad \mathbf{K} = \begin{bmatrix} -u_{3,11}^0 \\ -u_{3,22}^0 \\ -2u_{3,12}^0 \end{bmatrix}. \tag{22}$$

From these assumptions, we can calculate the dynamical bending equations for a piezoelectric laminated beam.

Appendix B gives the details of these calculations, and defines the quantities A^N, B^N, R, λ, $\boldsymbol{N}$, $\boldsymbol{M}$, P^D, Q^D, and J^D. We end up with the following expression for the electric charge displacement:

$$D_3 = P^D \varepsilon_{11}^0 + Q^D K_{11} + J^D E_3 \tag{23}$$

and two differential mechanical equations describing the longitudinal displacement u_1^0 and the transversal displacement u_3^0:

$$u_{1,11}^0 = \frac{B^N}{A^N} u_{3,111}^0, \tag{24}$$

$$R u_{3,1111}^0 - \lambda \omega^2 u_3^0 = 0. \tag{25}$$

Solutions of Eq. (25) can be written as

$$u_3^0(x_1) = a_1 \cos(\Omega x_1) + a_2 \sin(\Omega x_1) + a_3 \cosh(\Omega x_1) + a_4 \sinh(\Omega x_1), \tag{26}$$

with

$$\Omega^4 = \frac{\lambda \omega^2}{R}. \tag{27}$$

The solution of Eq. (24) is therefore

$$u_1^0(x_1) = \frac{\Omega B^N}{A^N}[-a_1 \sin(\Omega x_1) + a_2 \cos(\Omega x_1) + a_3 \sinh(\Omega x_1) + a_4 \cosh(\Omega x_1)] + a_5 x_1 + a_6, \tag{28}$$

a_1, a_2, a_3, a_4, a_5 and a_6 are constants calculated from the boundary conditions.

3.2. Accounting for the delamination using the transfer matrix method

As shown in Fig. 6, the beam is cut into several segments including all the various laminates. The aim here is to write kinematic and dynamic continuity conditions between each of the segments. First we replace in the expression for $u_3^0(x_1)$ and $u_1^0(x_1)$ the unknown coefficients a_1, a_2, a_3, a_4, a_5, and a_6 by the six kinematic node variables defined in Fig. 7, in order to automatically satisfy the kinematic continuity conditions.

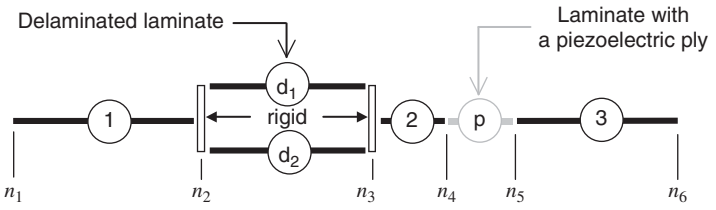

Fig. 6. Beam cutting.

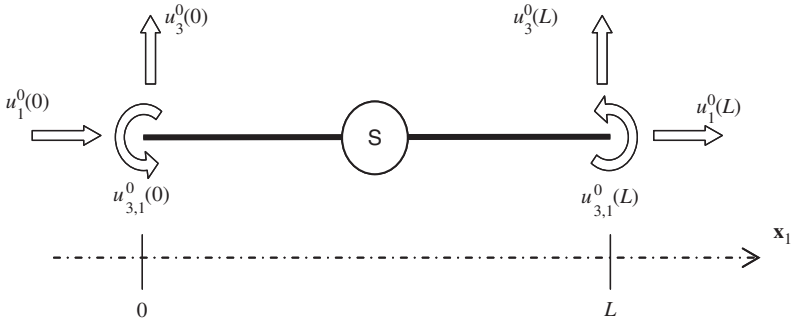

Fig. 7. Cinematic node variables.

The displacements $u_3^0(x_1)$ and $u_1^0(x_1)$ can therefore be written in the form:

$$u_3^0(x_1) = \begin{bmatrix} u_3^0(0) \\ u_3^0(L) \\ u_{3,1}^0(0) \\ u_{3,1}^0(L) \\ u_1^0(0) \\ u_1^0(L) \end{bmatrix}^{\mathrm{T}} \mathbf{CL}_3^{\mathrm{T}} \begin{bmatrix} \cos(\Omega x_1) \\ \sin(\Omega x_1) \\ \cosh(\Omega x_1) \\ \sinh(\Omega x_1) \\ x_1 \\ 1 \end{bmatrix}, \tag{29}$$

$$u_1^0(x_1) = \begin{bmatrix} u_3^0(0) \\ u_3^0(L) \\ u_{3,1}^0(0) \\ u_{3,1}^0(L) \\ u_1^0(0) \\ u_1^0(L) \end{bmatrix}^{\mathrm{T}} \mathbf{CL}_1^{\mathrm{T}} \begin{bmatrix} \cos(\Omega x_1) \\ \sin(\Omega x_1) \\ \cosh(\Omega x_1) \\ \sinh(\Omega x_1) \\ x_1 \\ 1 \end{bmatrix}. \tag{30}$$

Analytic expressions of $\mathbf{CL}_3$ and $\mathbf{CL}_1$ can be found in Ref. [22].

We can then express the dynamic equilibrium at each node: for example, let us write the equilibrium at node n_2:

$$N_{11}^1(n_2) = N_{11}^{d1}(n_2) + N_{11}^{d2}(n_2), \tag{31}$$

$$M_{11}^1(n_2) = M_{11}^{d1}(n_2) + M_{11}^{d2}(n_2), \tag{32}$$

$$M_{11,1}^1(n_2) = M_{11,1}^{d1}(n_2) + M_{11,1}^{d2}(n_2). \tag{33}$$

It is worth noting that the bending moments are all written at the same point; so the fact that each part of the beam has its own neutral fibre is taken into account.

Constitutive laws (64) and displacement fields (29) and (30) make it possible to express the dynamic equilibrium equations according to kinematic node variables. We thus obtain a $3n_n$ linear equations system where n_n is the number of nodes. By solving this system of equations, we can calculate the displacement fields depending on the electric potential V^+ of the positive terminal. The solution fields are proportional to the electric potential V^+ because the model is linear.

3.3. Admittance calculation

The transducer admittance is defined by

$$Y = \frac{I}{V^+}. \tag{34}$$

We calculate the electrical current I from the electric charge displacement:

$$I = \int_{+\text{ terminal}} \dot{D}_3 \, \mathrm{d}s = \mathrm{j}\omega \int_{+\text{ terminal}} D_3 \, \mathrm{d}s = \mathrm{j}\omega b \int_{n_p}^{n_p+1} D_3 \, \mathrm{d}x_1, \tag{35}$$

where n_p and n_{p+1} are the nodes at the transducer ends.

Eq. (23) can then be used to express I depending on the displacement field and the electrical field:

$$I = \mathrm{j}\omega b \int_{n_p}^{n_p+1} (P^D u^0_{1,1} - Q^D u^0_{3,11} + J^D E_3) \, \mathrm{d}x_1, \tag{36}$$

$$I = \mathrm{j}\omega b V^+ \left(P^D \Delta u^0_1 - Q^D \Delta u^0_{3,1} + J^D \frac{L_p}{h_p} \right), \tag{37}$$

where L_p is the length of the transducer, and Δu^0_1 and $\Delta u^0_{3,1}$ are defined by

$$\Delta u^0_1 = \frac{u^0_1(n_{p+1}) - u^0_1(n_p)}{V^+}, \quad \Delta u^0_{3,1} = \frac{u^0_{3,1}(n_{p+1}) - u^0_{3,1}(n_p)}{V^+}. \tag{38}$$

We can therefore express the admittance as follows:

$$Y = \mathrm{j}\omega \left[b(P^D \Delta u^0_1 - Q^D \Delta u^0_{3,1}) + J^D \frac{bL_p}{h_p} \right]. \tag{39}$$

As in the case of the general electromechanical model, we can see that the expression for the admittance contains an electrical term and a mechanical term. We can then express the total capacity C_T as follows:

$$C_T = b(P^D \Delta u^0_1 - Q^D \Delta u^0_{3,1}) + J^D \frac{bL_p}{h_p}. \tag{40}$$

4. Characterisation of the delamination by parametric identification

Characterisation of a defect using a parametric identification procedure requires the use of three tools:

- An efficient model reducing the computation time.
- A smooth cost function for quantifying the difference between experiments and simulations.
- A fast and reliable minimisation algorithm.

To obtain the first tool, we used the model presented in the previous part. This model accounts for both the delamination and the transducer. Three parameters have to be identified: the length, the position, and the depth of the delamination.

To define the cost function, we compared the modal parameters of a few modes of the structure between experiments and simulations. The first step consisted in extracting the modal parameters from the electromechanical impedance. Next, a cost function based on resonance frequencies and mode amplitudes yielded a robust identification procedure. We used a quadratic cost function, which had a single minimum for all the cases that we considered, so we did not need to develop a specific minimisation algorithm as required in other work [18].

4.1. Extracting modal parameters from electromechanical impedance measurements

The first stage in the procedure consists in analysing the admittance in order to obtain the modal response of the structure and extract the modal parameters involved in each mode.

We assume each mode to be independent from the others, so that each mode is assimilated to a one dof mechanical system. In the example presented in Fig. 2 this assumption is acceptable at frequencies lower than 10 kHz.

A 1 dof mechanical system of this kind is presented in Fig. 8. Eq. (8) can be used to calculate the expression for the electrical admittance in the case of this simple system:

$$Y = j\omega[P(k + j\omega k^* - \omega^2 m)^{-1} P + C]. \tag{41}$$

In this case, since P is a scalar, Eq. (41) gives

$$Y - j\omega C = P^2 \frac{j\omega}{k + j\omega k^* - \omega^2 m}. \tag{42}$$

This expression includes the mechanical admittance of a 1 dof mechanical system defined by

$$Y_m = \frac{\dot{U}}{F} = \frac{j\omega}{k + j\omega k^* - \omega^2 m}. \tag{43}$$

We can therefore now identify the modal parameters of each mode: the resonance frequency f_r, the quality factor Q, and the amplitude A, defined by

$$f_r = \frac{1}{2\pi}\sqrt{\frac{k}{m}}, \quad Q = \frac{2\pi f_r m}{k^*}, \quad \text{and} \quad A = \frac{1}{k^*}. \tag{44}$$

For this purpose, we use a high resolution technique developed by Le Roux and Herzog [32] based on a least squares identification method. This method is based on an analytic solution, which makes it possible to accurately estimate modal parameters, even with highly damped resonances. Fig. 9 gives the third mode identified in the spectrum shown in Fig. 2. The total experimental capacity and its identification can be compared in Fig. 10 and seem to be in excellent agreement. Since C varies slightly with the frequency, we have plotted in Figs. 9 and 10 the evolution of C_d, which is the difference between C_T and its static value.

4.2. Application to the characterisation of delaminations

The laminate studied here consisted of 16 unidirectional carbon/epoxy plies with the sequence $[45°, -45°, 90°, 0°]_{2S}$. Six transducers were cemented to the beam with cyanoacrylate as shown in Fig. 11. We used piezoelectric transducers obtained from inexpensive electronic buzzers, made of a 0.15 mm thick PZT ply and a 0.2 mm thick steel ply. The characteristics of the materials are given in Table 1.

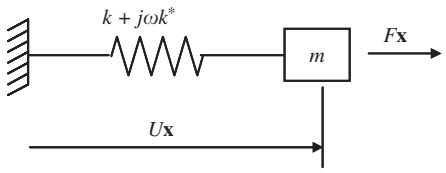

Fig. 8. One degree of freedom mechanical system.

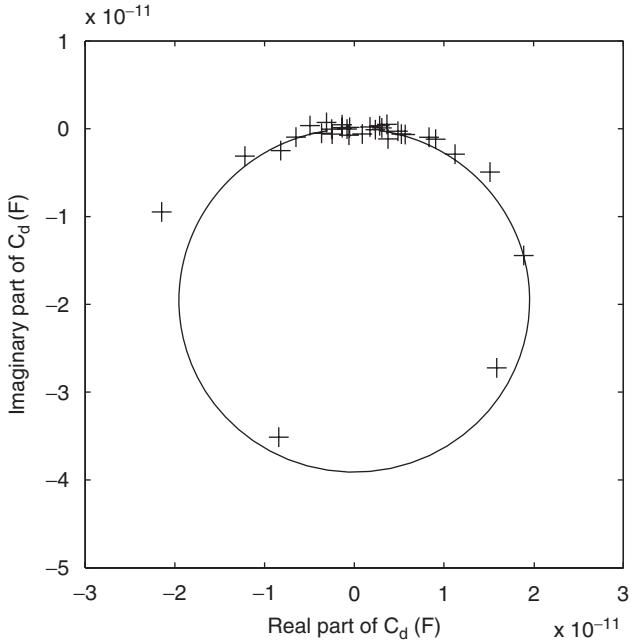

Fig. 9. Identification of the third mode of the spectrum corresponding to Fig. 2. +, experimental points; —, identification.

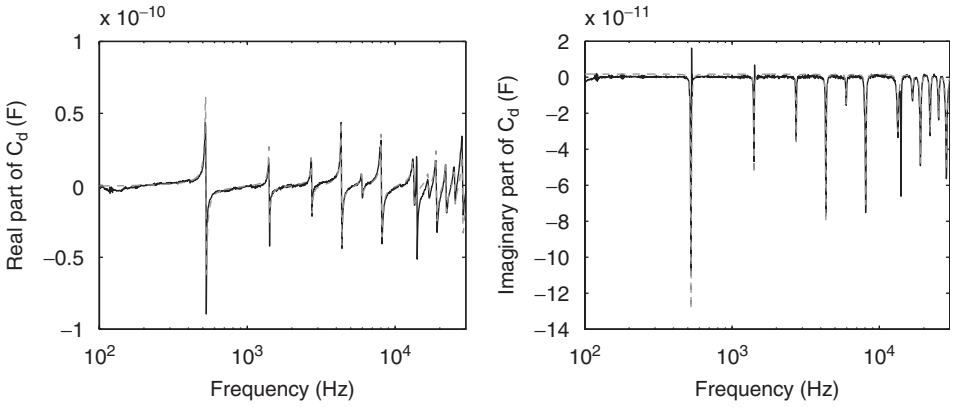

Fig. 10. Comparison between experimental total capacity and its identification. —, measurement; - - -, identification.

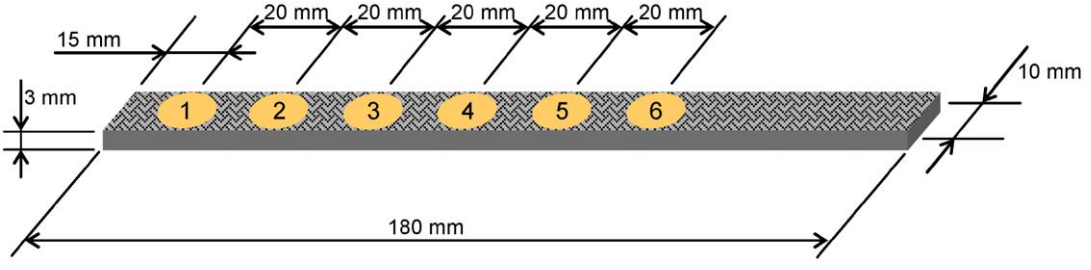

Fig. 11. Studied beam.

Table 1
Material properties

Material properties	Composite measured data	Piezoelectric (PZT) (see Ref. [33])	Steel
Elastic properties	$E_1/E_2/G_{12}/\nu_{12}$	$E_1/E_2/\nu_{12}$	E/ν
(Gpa)	135/9/4/0.33	64.5/64.5/0.3	210/0.3
Damping coefficient: ξ	$\xi_1/\xi_2/\xi_{12}$	$\xi_1/\xi_2/\xi_{12}$	ξ
$E^* = E(1+j\xi)$	0.002/0.02/0.03	0.001/0.001/0.001	0.001
Mass density (kg/m^3)	1600	7500	7800
Permitivity: ε_{33} (C/m/V)	—	6.9×10^{-9}	—
Coupling term: d_{113} and d_{223} (m/V)	—	-5.54×10^{-11}	—

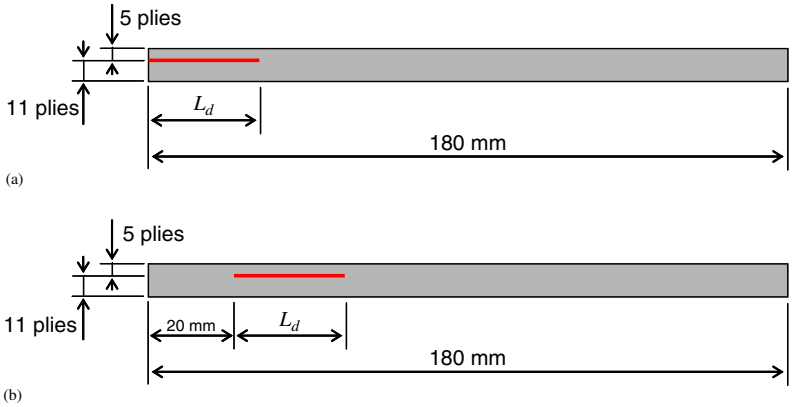

Fig. 12. Configurations of studied delamination. (a) Delamination at one end of the beam. (b) Delamination located inside the beam.

The delamination is introduced between the 11th and 12th plies because $0^\circ/90^\circ$ interface is brittle with respect to delamination. The process is initiated by an unmoulding plastic film and increased using a very thin blade. Two patterns of delamination were studied: one starting at one end of the beam, and the other one occurring entirely inside the beam (Fig. 12).

The laminate was placed on two soft foam blocks in order to approximate free boundary conditions.

Measurements were performed with a Stanford spectrum analyser. The simulation was programmed in Matlab® on a computer with a 2 GHz processor and 512 Mo RAM. The computation time required to process 300 frequency values was about 1 s.

The frequency range investigated, 100 Hz–30 kHz, was chosen in order to include the first bending modes.

Several cost functions were tested, some of which were based only on resonance frequencies, and some only on mode amplitudes. The final cost function was based on both resonance frequencies and mode amplitudes:

$$Fc = \sqrt{\sum_{i=1}^{4}\left(\frac{f_{ri}^{\text{measured}} - f_{ri}^{\text{simulated}}}{f_{ri}^{\text{measured}}}\right)^2} + \sqrt{\sum_{i=1}^{4}\left(\frac{A_i^{\text{measured}} - A_i^{\text{simulated}}}{A_i^{\text{measured}}}\right)^2}. \tag{45}$$

The first four modes yielded a sufficiently large amount of information, while requiring a reasonable computation time.

The results presented below were obtained using the 5th transducer, which was not placed near the region of delamination. We checked that the delamination identification method worked with each of the six transducers used: the amplitudes of the peaks in the impedance curves obtained with all the transducer were very similar on the whole (see Ref. [22]). The reason for this similarity is that the global modes of the structure reflect the defect, and can therefore be used to characterise it wherever the transducer is positioned, provided that (as in our case) the size of the damage is significant in comparison with the size of the structure.

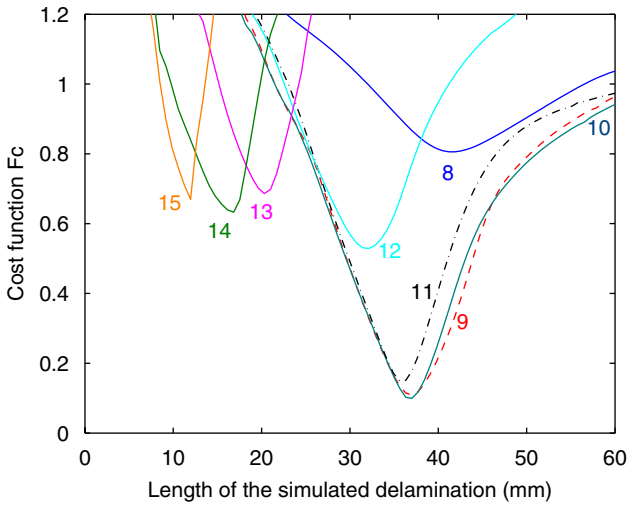

Fig. 13. Evolution of the cost function *Fc* for a 42 mm long delamination. Transducer #5. Each interface number is written close of the corresponding curve.

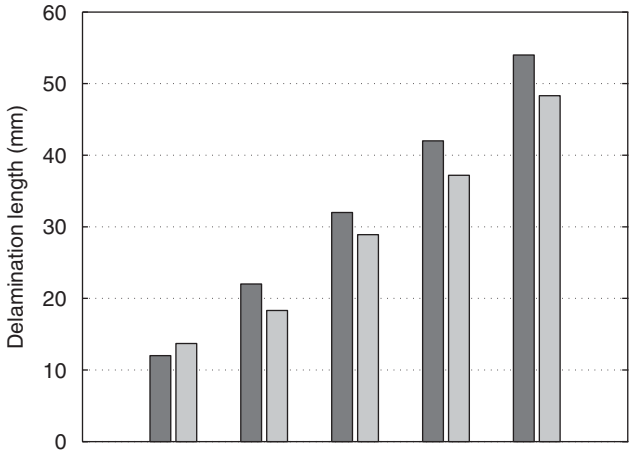

Fig. 14. Comparison between identified lengths and actual lengths. Transducer #5. , actual length; , identified length.

4.2.1. Delamination at one end of the beam

In this case, only two parameters are used to characterise the delamination: the length and the depth of the delaminated interface. Fig. 13 shows the influence of the length of the simulated delamination on the cost function. The length of the actual delamination was 42 mm and the transducer used was number 5. At each delaminated interface, there is a clearly identifiable minimum which corresponds to a delamination length. Interface numbers 9, 10, and 11 give the lowest minima and similar results: the length of the delamination identified in all these cases was 37 mm. The identified length can be compared with the actual length in Fig. 14. The simulated delamination length using our method was underestimated by 10%, possibly due to the presence of an adherence zone at the end of the delamination zone.

4.2.2. Delamination located inside the beam

In this case, three parameters can be said to characterise the delamination: the length, the position, and the depth. Fig. 15 shows the influence of the length of the simulated delamination on the cost function when the depth of the delaminated interface was fixed. The actual delamination length was 32 mm, the distance between

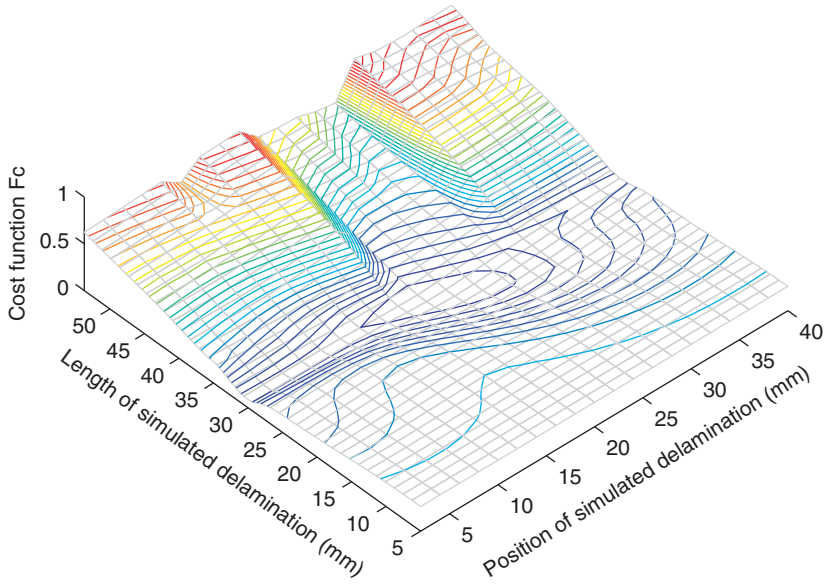

Fig. 15. Evolution of the cost function Fc for a 32 mm long delamination. Transducer #5.

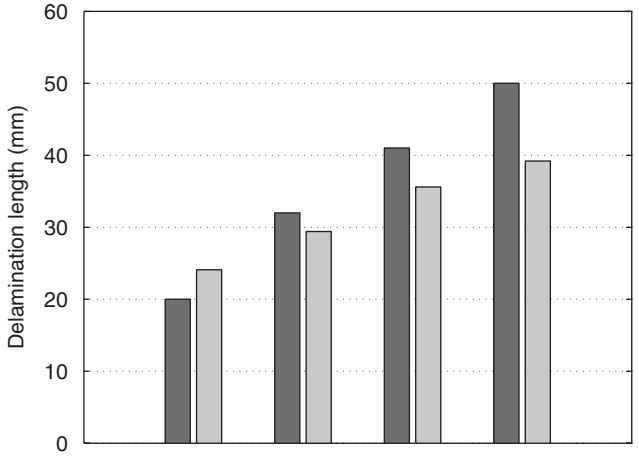

Fig. 16. Comparison between identified lengths and actual lengths. Transducer #5. ■, actual length ; ▪▪▪, identified length.

the end of the beam and the end of the delamination zone was 20 mm, and the transducer used was number 5. The cost function shows a clearly detectable minimum, which correspond to a 29.4 mm long delamination and a distance of 20 mm between the end of the beam and the end of the delamination.

The identified lengths and actual lengths can be compared in Fig. 16. The simulated delamination length was underestimated by 15% possibly due to the presence of two adherence zones at the beginning and end of the delamination zone. It can be seen from Fig. 17 that the site at which the delamination occurred was accurately estimated.

5. Conclusion and prospects

An in-situ method of measurement is described here for detecting and characterising a delamination process in a composite structure. The method was applied to a beam structure. For this purpose, we developed an

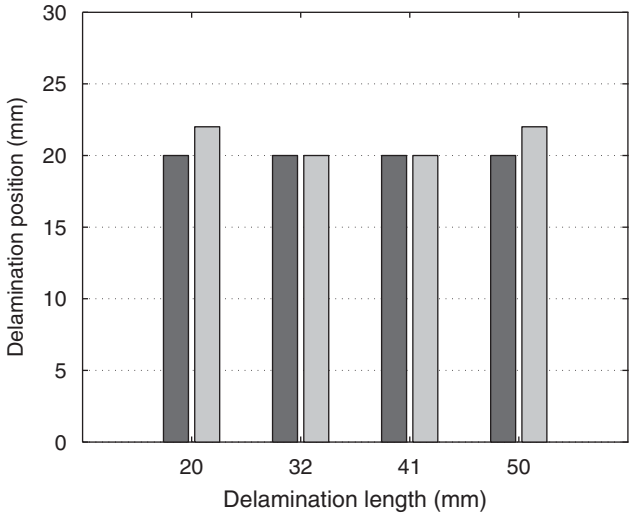

Fig. 17. Comparison between identified positions and actual positions. Transducer #5. ■, actual length ; ▪▪▪, identified length.

analytic model for a beam including a delaminated part and a transducer. Modal parameters were obtained from the electromechanical impedance measurements and from simulations. These parameters were then compared in order to determine the most appropriate model parameters. The size and position of the defect were found to be accurately estimated in the cases tested, where the delamination was a large one (about 10% of the total length of the structure).

Our research team is also working on the use of similar methods to detect micro-crack processes. The initial results obtained show that damage of this kind does not significantly affect the modal parameters in the frequency range used here to detect a delamination. The delamination monitoring will therefore probably not be disturbed if multiple damage occurs in a composite material. However, this has not yet been checked.

The detection range of a single sensor depends on the characteristics of the structure involved (its dimensions, the boundary conditions, etc.), on the delamination configuration (open or closed), and on the type of coupling which occurs. The latest simplified model could now be used to study the effects of these parameters, and it is already a good candidate for dealing with a few specific industrial problems. In the first stage, it is proposed to use this method to detect a delamination on the trailing edge of a helicopter blade: the dynamic behaviour of this slim structure is quite simple, and the delamination usually propagates only along the trailing edge. A 1D model should therefore suffice to deal with this problem.

Most industrial applications cannot be solved using 1D model, however. 2D models require a numerical method, such as the finite elements method. Some authors have developed models including either a delamination or a piezoelectric transducer, and we are also developing a finite element model based on the discrete kirchhoff triangular (DKT) element procedure accounting for both the transducer and the delamination. Obtaining an accurate and time-saving model is not the only problem which requires to be solved. In the case of a 2D structure, the difficulty of characterising the delamination will depend on the mode density and the coupling between the various modes.

Appendix A. Discretised equations for the electromechanical problem

Let us take $\boldsymbol{\sigma}$ to denote the Cauchy stress tensor, $\mathbf{u}$ the displacement vector, and $\boldsymbol{\varepsilon}$ the strain tensor defined by

$$\varepsilon_{ij} = \tfrac{1}{2}(u_{i,j} + u_{j,i}). \tag{46}$$

In the variational form, the global mechanical equilibrium equation is

$$-\int_{\Omega}\sigma_{ij}\delta\varepsilon_{ij}\,\mathrm{d}v=\int_{\Omega}\rho\,\frac{\mathrm{d}^2u_i}{\mathrm{d}t^2}\delta u_i\,\mathrm{d}\Omega\quad\forall\delta\mathbf{u},\tag{47}$$

where ρ is the density and $\delta\mathbf{u}$ the virtual displacement.

In the variational form, the global electrical equilibrium equation is

$$\int_{\Omega_p}D_p\delta E_p\,\mathrm{d}v-\int_{+\text{ terminal}}Q\delta V\,\mathrm{d}v=0\quad\forall\delta V,\tag{48}$$

where Q is a surface electric charge displacement and δV the virtual electric potential.

Using $\boldsymbol{\varepsilon}$ and $\mathbf{E}$ as independent variables, the constitutive laws become:

$$D_p=e_{pkl}\varepsilon_{kl}+\varepsilon^{\varepsilon}_{pq}E_q,\tag{49}$$

$$\sigma_{ij}=K^{E}_{ijkl}\varepsilon_{kl}-e_{ijq}E_q,\tag{50}$$

where $\boldsymbol{\varepsilon}^{\varepsilon}$ is the dielectric tensor at constant strain field, $\mathbf{K}^{E}$ is the stiffness tensor at constant electrical field, and $\mathbf{e}$ is the corresponding piezoelectric coupling tensor.

We thus obtain the following global expressions solving the piezoelectric structure problem:

$$-\int_{\Omega}K^{E}_{ijkl}\varepsilon_{kl}\delta\varepsilon_{ij}\,\mathrm{d}v+\int_{\Omega_p}e_{ijq}E_q\delta\varepsilon_{ij}\,\mathrm{d}v=\int_{\Omega}\rho\,\frac{\mathrm{d}^2u_i}{\mathrm{d}t^2}\delta u_i\,\mathrm{d}\Omega\quad\forall\delta\mathbf{u},\tag{51}$$

$$\int_{\Omega_p}e_{pkl}\varepsilon_{kl}\delta E_p\mathrm{d}v+\int_{\Omega_p}\varepsilon^{\varepsilon}_{pq}E_q\delta E_p\,\mathrm{d}v-\int_{+\text{ terminal}}Q\delta V\,\mathrm{d}v=0\quad\forall\delta V.\tag{52}$$

To express the admittance literally, let the displacement field discretised using the finite elements method:

$$u_i(x_1,x_2,x_3)=\sum_{p=1}^{n}N^p(x_1,x_2,x_3)U^p_i,\tag{53}$$

where U^p_i indicates the displacement of the node numbered p in the $\mathbf{x}_i$ direction, N^p the base function of the node numbered p, and n the number of nodes.

To deal with the electric potential let us use the approximate forms of Eqs. (3) and (4).

In this way, we obtain the following equation:

$$\begin{cases}(\mathbf{K}-\omega^2\mathbf{M})\mathbf{U}-\mathbf{P}V^{+}=0,\\ \mathbf{P}^{\mathrm{T}}\mathbf{U}+CV^{+}=\dfrac{I}{\mathrm{j}\omega},\end{cases}\tag{54}$$

where $\mathbf{U}$ is the column vector of nodal displacements, $\mathbf{K}$ the stiffness matrix, $\mathbf{M}$ the mass matrix, $\mathbf{P}$ the column vector of electromechanical coupling, and C the electric capacity. C is defined by

$$C=\frac{S\varepsilon^{\varepsilon}_{33}}{h_p},\tag{55}$$

where S is the area of the positive terminal.

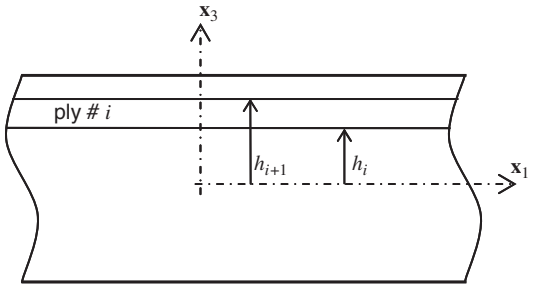

Fig. 18. Laminate description.

Appendix B. Theory for a piezoelectric laminate—Application to a laminated beam

We start calculating generalised forces: the axial and moment forces are defined by

$$\begin{cases} \mathbf{N} = \displaystyle\int_{h_1}^{h_{n+1}} \boldsymbol{\sigma}\,\mathrm{d}x_3 = \sum_{i=1}^{n}\left(\int_{h_i}^{h_{i+1}} \boldsymbol{\sigma}\,\mathrm{d}x_3\right), \\ \mathbf{M} = \displaystyle\int_{h_1}^{h_{n+1}} \boldsymbol{\sigma} x_3\,\mathrm{d}x_3 = \sum_{i=1}^{n}\left(\int_{h_i}^{h_{i+1}} \boldsymbol{\sigma} x_3\,\mathrm{d}x_3\right), \end{cases} \tag{56}$$

where n is the number of plies. h_i and h_{i+1} are defined in Fig. 18.

Using the constitutive law (18), we obtain

$$\begin{cases} \mathbf{N} = \displaystyle\int_{h_1}^{h_{n+1}} (\mathbf{S}^E)^{-1}\boldsymbol{\varepsilon}\,\mathrm{d}x_3 - \int_{h_1}^{h_{n+1}} (\mathbf{S}^E)^{-1}\,\mathbf{d}E_3\,\mathrm{d}x_3, \\ \mathbf{M} = \displaystyle\int_{h_1}^{h_{n+1}} (\mathbf{S}^E)^{-1}\boldsymbol{\varepsilon} x_3\,\mathrm{d}x_3 - \int_{h_1}^{h_{n+1}} (\mathbf{S}^E)^{-1}\,\mathbf{d}E_3 x_3\,\mathrm{d}x_3. \end{cases} \tag{57}$$

Using Kirchhoff–Love's displacement field summarised in Eq. (21), Eq. (57) gives

$$\begin{cases} \mathbf{N} = \mathbf{A}\,\boldsymbol{\varepsilon}^0 + \mathbf{B}\mathbf{K} - \mathbf{F}E_3, \\ \mathbf{M} = \mathbf{B}\,\boldsymbol{\varepsilon}^0 + \mathbf{D}\mathbf{K} - \mathbf{G}E_3, \end{cases} \tag{58}$$

with

$$\begin{aligned} &\mathbf{A} = \sum_{i=1}^{n}(\mathbf{S}_i^E)^{-1}(h_{i+1}-h_i), \quad \mathbf{B} = \sum_{i=1}^{n}(\mathbf{S}_i^E)^{-1}\frac{h_{i+1}^2 - h_i^2}{2}, \\ &\mathbf{D} = \sum_{i=1}^{n}(\mathbf{S}_i^E)^{-1}\frac{h_{i+1}^3 - h_i^3}{3}, \quad \mathbf{F} = (h_{p+1}-h_p)(\mathbf{S}_p^E)^{-1}\mathbf{d}, \\ &\text{and} \quad \mathbf{G} = \frac{h_{p+1}^2 - h_p^2}{2}(\mathbf{S}_p^E)^{-1}\mathbf{d}, \end{aligned} \tag{59}$$

where p is the index of the piezoelectric ply.

We can proceed in the same way with Eq. (19):

$$D_3 = \mathbf{d}^{\mathrm{T}}(\mathbf{S}_p^E)^{-1}(\boldsymbol{\varepsilon}^0 + x_3\mathbf{K}) + (\varepsilon_{33}^{\sigma} - \mathbf{d}^{\mathrm{T}}(\mathbf{S}_p^E)^{-1}\mathbf{d})E_3. \tag{60}$$

We can see here that D_3 depend on x_3, which is incompatible with our starting assumptions. In fact, the electrical equilibrium given by Eq. (48) cannot be exactly satisfied. However, the piezoelectric layer is thin and this dependence is weak. We can therefore take as an approximation the average displacement of the electric

charges in direction x_3:

$$D_3 = \mathbf{d}^{\mathrm{T}}(\mathbf{S}^E)^{-1}\left(\boldsymbol{\varepsilon}^0 + \frac{h_{p+1}+h_p}{2}\,\mathbf{K}\right) + (\varepsilon_{33}^{\sigma} - \mathbf{d}^{\mathrm{T}}(\mathbf{S}^E)^{-1}\mathbf{d})E_3. \tag{61}$$

Our aim is now to study the bending modes of a beam in the plane ($\mathbf{x}_1$, $\mathbf{x}_3$). For this purpose, we seek solutions where only the forces in the $\mathbf{x}_1$ direction are not equal to zero, what gives

$$N_{22} = 0, \quad M_{22} = 0, \quad N_{12} = 0 \quad \text{and} \quad M_{12} = 0. \tag{62}$$

Of course, in the case of most laminates, there are interactions between different directions, and so ε_{22}^0, K_{22}, ε_{12}^0, and K_{12} are generally not equal to zero. In fact, the conditions given by Eq. (62) and the constitutive relations given by Eq. (58) make it possible to calculate these strains in terms of ε_{11}^0, K_{11}, and E_3.

In only remains now to solve the following equation:

$$\begin{bmatrix} A_{22} & B_{22} & A_{23} & B_{23} \\ B_{22} & D_{22} & B_{23} & D_{23} \\ A_{32} & B_{32} & A_{33} & B_{33} \\ B_{32} & D_{32} & B_{33} & D_{33} \end{bmatrix} \begin{bmatrix} \varepsilon_{22}^0 \\ K_{22} \\ \varepsilon_{12}^0 \\ K_{12} \end{bmatrix} = \begin{bmatrix} -A_{12}\varepsilon_{11}^0 - B_{12}K_{11} + F_2E_3 \\ -B_{12}\varepsilon_{11}^0 - D_{12}K_{11} + G_2E_3 \\ -A_{13}\varepsilon_{11}^0 - B_{13}K_{11} + F_3E_3 \\ -B_{13}\varepsilon_{11}^0 - D_{13}K_{11} + G_3E_3 \end{bmatrix}. \tag{63}$$

In this way, we obtain N_{11} and M_{11} in terms of ε_{11}^0, K_{11}, and E_3:

$$\begin{cases} N_{11} = A^N\varepsilon_{11}^0 + B^NK_{11} - F^NE_3, \\ M_{11} = B^M\varepsilon_{11}^0 + D^MK_{11} - G^ME_3. \end{cases} \tag{64}$$

We can proceed in the same way with Eq. (61):

$$D_3 = P^D\varepsilon_{11}^0 + Q^DK_{11} + J^DE_3. \tag{65}$$

Coefficients A^N, B^N, F^N, B^M, D^M, G^M, P^D, Q^D, and J^D are numerically calculated.

Let us now determine the differential equation of movement. For this purpose, let us use the dynamical equilibrium equations given by the Kirchhoff–Love's plate theory:

$$\begin{cases} N_{11,1} + N_{12,2} - \lambda u_{1,tt}^0 = 0, \\ N_{22,2} + N_{12,1} - \lambda u_{2,tt}^0 = 0, \\ M_{11,11} + M_{22,22} + M_{12,12} - \lambda u_{3,tt}^0 = 0, \end{cases} \tag{66}$$

where λ is the surface density:

$$\lambda = \sum_{i=1}^{n} \rho_i(h_{i+1} - h_i). \tag{67}$$

We seek the solutions for similar frequencies to those occurring in the relatively low frequency bending modes. Since the angular frequency of the first bending mode is much lower than that of the first axial mode, we can neglect the inertial forces in directions $\mathbf{x}_1$ and $\mathbf{x}_2$:

$$\begin{cases} N_{11,1} + N_{12,2} = 0, \\ N_{22,2} + N_{12,1} = 0, \\ M_{11,11} + M_{22,22} + M_{12,12} + \lambda\omega^2 u_3^0 = 0. \end{cases} \tag{68}$$

With the conditions given by Eq. (62), Eq. (68) becomes

$$\begin{cases} N_{11,1} = 0, \\ M_{11,11} + \lambda\omega^2 u_3^0 = 0. \end{cases} \tag{69}$$

Let us substitute Eq. (64) into Eq. (69):

$$\begin{cases} A^N u^0_{1,11} - B^N u^0_{3,111} - F^N E_{3,1} = 0, \\ B^M u^0_{1,111} - D^M u^0_{3,1111} - G^M E_{3,11} + \lambda\omega^2 u^0_3 = 0. \end{cases} \tag{70}$$

Since we have assumed that E_3 does not depend on x_1, we obtain

$$\begin{cases} A^N u^0_{1,11} - B^N u^0_{3,111} = 0, \\ B^M u^0_{1,111} - D^M u^0_{3,1111} + \lambda\omega^2 u^0_3 = 0. \end{cases} \tag{71}$$

Let us note that if the laminate is symmetrical, B^N and B^M will be equal to zero and Eq. (71) will be uncoupled (there will be no coupling between flexion and tension). However, in the delaminated zone or in the piezoelectric zone, dissymmetry is unavoidable.

Let us uncouple the system of equations in Eq. (71) by using the first equation of this system:

$$u^0_{1,11} = \frac{B^N}{A^N} u^0_{3,111}. \tag{72}$$

Substituting into the second equation of the system, we obtain

$$R u^0_{3,1111} - \lambda\omega^2 u^0_3 = 0, \tag{73}$$

with

$$R = D^M - \frac{B^N B^M}{A^N}. \tag{74}$$

References

[1] P. Ladevèze, A damage computational method for composite structures, *Computers and Structures* 44 (1–2) (1992) 79–87.

[2] S.W. Tsaï, *Composites Design, Think Composites*, fourth ed., Dayton, 1988.

[3] M.M. Shokrieh, L.B. Lessard, Progressive fatigue damage modeling of composite materials, part I: Modeling, *Journal of Composite Materials* 34 (13) (2000) 1056–1080.

[4] T. Monnier, et al., The piezoelectric implant method: implementation and practical applications, *Smart Materials and Structures* 9 (3) (2000) 267–272.

[5] A. Todoroki, Y. Tanaka, Delamination identification of cross-ply graphite/epoxy composite beams using electric resistance change method, *Composites Science and Technology* 62 (5) (2002) 629–639.

[6] J.C. Abry, et al., In-situ monitoring of damage in CFRP laminates by means of AC and DC measurements, *Composites Science and Technology* 61 (6) (2001) 855–864.

[7] D.D.L. Chung, Structural health monitoring by electrical resistance measurement, *Smart Materials and Structures* 10 (4) (2001) 624–636.

[8] D.C. Lee, et al., Monitoring of fatigue damage of composite structures by using embedded intensity-based optical fibre sensors, *Smart Materials and Structures* 10 (2) (2001) 285–292.

[9] D. Balageas, et al., Comparison between non-destructive evaluation techniques and integrated fibre optic health monitoring systems for composite sandwich structures, *Journal of Intelligent Material Systems and Structures* 11 (6) (2000) 426–437.

[10] M. Lin, F.-K. Chang, The manufacture of composite structures with a built-in network of piezoceramics, *Composites Science and Technology* 62 (7–8) (2002) 919–939.

[11] P. Cawley, D. Alleyne, The use of Lamb waves for the long range inspection of large structures, *Ultrasonics* 34 (2–5) (1996) 287–290.

[12] S. Grondel, et al., Fatigue crack monitoring of riveted aluminium strap joints by Lamb wave analysis and acoustic emission measurement techniques, *NDT&E international* 35 (3) (2002) 137–146.

[13] S.W. Doebling, C.R. Farrar, M.B. Prime, A summary review of vibration-based damage identification methods, *The Shock and Vibration Digest* 30 (2) (1998) 91–105.

[14] R.F. Gibson, Modal vibration response measurement for characterization of composite materials structures, *Composites Science and Technology* 60 (15) (2000) 2769–2780.

[15] R.M. Gadelrab, The effect of delamination on the natural frequencies of a laminated composite beam, *Journal of Sound and Vibration* 197 (3) (1996) 283–292.

[16] S. Prabhakar, A.S. Sekhar, A.R. Mohanty, Detection and monitoring of cracks using mechanical impedance of rotor-bearing system, *Journal of Acoustical Society of America* 110 (5) (2001) 2351–2359.

[17] S.H. Diaz Valdes, C. Soutis, Delamination detection in composite laminates from variations of their modal characteristics, *Journal of Sound and Vibration* 228 (1) (1999) 1–9.
[18] H.-Y. Ling, K.-T. Lau, L. Cheng, W. Jin, Fiber optic sensors for delamination identification in composite beams using a genetic algorithm, *Smart Material and Structures* 14 (1) (2005) 287–295.
[19] C.H. Keilers, F.-K. Chang, Identifying delamination in composites beams using built-in piezoelectrics: Part I—Experiments and analysis, *Journal of Intelligent Material Systems and Structures* 6 (5) (1995) 649–663.
[20] C.H. Keilers, F.-K. Chang, Identifying delamination in composites beams using built-in piezoelectrics: Part II—An identification method, *Journal of Intelligent Material Systems and Structures* 6 (5) (1995) 664–672.
[21] S.-F. Ling, Y. Xie, Detecting mechanical impedance of structures using the sensing capability of piezoceramic inertial actuator, *Sensors and Actuators A: Physical* 93 (3) (2001) 243–249.
[22] C. Bois, Mesure et prévision de l'évolution des endommagements dans les composites stratifiés. Ph.D. Thesis, Université de la Méditerranée, Laboratoire de Mécanique et d'Acoustique, Marseille, France, 2003. Available on ⟨http://tel.ccsd.cnrs.fr/⟩.
[23] S.V. Gopinathan, V.V. Varadan, V.K. Varadan, A review and critique of theories for piezoelectric laminates, *Smart Materials and Structures* 9 (1) (2000) 24–48.
[24] Q. Wang, S.T. Quek, A model for the analysis of beams with embedded piezoelectric layers, *Journal of Intelligent Material Systems and Structures* 13 (1) (2002) 61–70.
[25] F. Lalande, Z. Chaudhry, C.A. Rogers, Impedance-based modelling of actuators bounded to shell structures, *Journal of Intelligent Material Systems and Structures* 6 (6) (1995) 765–775.
[26] V. Giurgiutiu, A.N. Zagrai, Characterisation of piezoelectric wafer active sensors, *Journal of Intelligent Material Systems and Structures* 11 (12) (2001) 959–976.
[27] M. Rahmoune, et al., New thin piezoelectric plate models, *Journal of Intelligent Material Systems and Structures* 9 (12) (1998) 1017–1029.
[28] P. Tan, L. Tong, Delamination detection of composite beams using piezoelectric sensors with evenly distributed electrode strips, *Journal of Composite Materials* 38 (4) (2004) 321–352.
[29] Y. Zou, L. Tong, G.P. Steven, Vibration-based model-dependent damage (delamination) identification and health monitoring for composite structures: a review, *Journal of Sound and Vibration* 230 (2) (2000) 357–378.
[30] M. Cho, J.S. Kim, Higher-order zig-zag theory for laminated composites with multiple delaminations, *Journal of Applied Mechanics* 68 (6) (2001) 869–877.
[31] C. Bois, C. Hochard, Monitoring of laminated composites delamination based on electro-mechanical impedance measurement, *Journal of Intelligent Material Systems and Structures* 15 (1) (2004) 59–67.
[32] J.C. Le Roux, P. Herzog, Effect of suspension on electrodynamic loudspeaker. In: Proceedings of the 31st Conference on Acoustics, Prague, 1994.
[33] I.R. Henderson, *Piezoelectric ceramics: properties & applications*, APC International, Mackeyville, USA, 2002.